SCIENTIFIC REPORTS

OPEN

SUBJECT AREAS:
PHOTOCATALYSIS
SYNTHESIS

Received
18 December 2013

Accepted
13 January 2014

Published
5 February 2014

Correspondence and requests for materials should be addressed to L.S.Z. (lszhang@dhu.edu.cn) or J.S.L. (liujianshe@dhu.edu.cn)

Ta_3N_5-Pt nonwoven cloth with hierarchical nanopores as efficient and easily recyclable macroscale photocatalysts

Shijie Li[1], Lisha Zhang[1], Huanli Wang[1], Zhigang Chen[2], Junqing Hu[2], Kaibing Xu[2] & Jianshe Liu[1]

[1]College of Environmental Science and Engineering, Donghua University, [2]State Key Laboratory for Modification of Chemical Fibers and Polymer Materials, College of Materials Science and Engineering, Donghua University, Shanghai 201620, People's Republic of China.

Traditional nanosized photocatalysts usually have high photocatalytic activity but can not be efficiently recycled. Film-shaped photocatalysts on the substrates can be easily recycled, but they have low surface area and/or high production cost. To solve these problems, we report on the design and preparation of efficient and easily recyclable macroscale photocatalysts with nanostructure by using Ta_3N_5 as a model semiconductor. Ta_3N_5-Pt nonwoven cloth has been prepared by an electrospinning-calcination-nitridation-wet impregnation method, and it is composed of Ta_3N_5 fibers with diameter of 150–200 nm and hierarchical pores. Furthermore, these fibers are constructed from Ta_3N_5 nanoparticles with diameter of ~25 nm which are decorated with Pt nanoparticles with diameter of ~2.5 nm. Importantly, Ta_3N_5-Pt cloth can be used as an efficient and easily recyclable macroscale photocatalyst with wide visible-light response, for the degradation of methylene blue and parachlorophenol, probably resulting in a very promising application as "photocatalyst dam" for the polluted river.

Environmental problems associated with harmful pollutants in water pose severe threats to human health. Among the water treating methods, photocatalysis offers a "green" and energy saving technology for completely eliminating organic pollutants in water[1–3]. A prerequisite for the development of photocatalysis application is to gain access to excellent photocatalysts. Generally, two kinds of photocatalysts have been well developed. One kind is the nanosized semiconductor photocatalysts, including nanoparticles[4], nanotubes[5], nanowires[6], nanosheets[7], nanospheres[8] and nanocomposites[9–11]. Recently, we have also prepared some nanosized photocatalysts, such as Bi_2WO_6 superstructures[12,13], and AgBr-Ag-Bi_2WO_6 nanojunction system[14]. They always show relatively high photocatalytic activity due to their nanoscaled particle size and large specific surface area. Unfortunately, it is very difficult to recycle these nanosized photocatalysts in practical application (such as degrading organic pollutants in lake and/or river), resulting in second-contamination and limiting their large-scale application. The other kind is semiconductor films on the substrates, such as nanoparticles-based composite films on ITO glass[15,16], nanowires/nanotubes-based film grew on metal foil[17,18]. These film-shaped photocatalysts on the substrate can be easily recycled, but they suffer from the problems, such as relatively low surface area and/or high production cost. Thus, it is quite necessary to develop novel kind of photocatalysts. Ideal photocatalysts should have a broad range of visible-light response, superior photocatalytic activity, high photostability, low cost and easily recycling characteristics, and etc.

It is well known that micro/nano-fibers and nonwoven cloth can be easily prepared via electrospinning technique that represents a simple, cost-effective and versatile method for the large-scale production of fibers. Traditional micro/nano-fibers are polymer or polymer/inorganic composite fibers[19–21]. Few kinds of semiconductor nanofibers including TiO_2[22], $Bi_4Ti_3O_{12}$[23], TiO_2/SnO_2[24] and GaN[25] have been prepared for photocatalysis or photodetector. In photocatalytic application, semiconductor nanofibers have also suffered from the problems such as relatively low surface area and recycle difficulty. It should be noted that macroscale nonwoven cloth are usually composed of polymer or polymer/inorganic composite fibers, and they have already found use in applications (such as drug carriers, tissue engineering and ultrafiltration) and can be easily recycled. If semiconductor nonwoven cloth is composed of nanofibers that are constructed from semiconductor nanoparticles

with plenty of hierarchical nanopores, it will have both high surface area and easily recycling characteristics for photocatalytic application. These features trigger our interest in the novel concept of developing efficient and easily recyclable macroscale semiconductor photocatalysts with nanostructure.

Among semiconductor photocatalysts, Ta_3N_5 with a narrow band gap of approximately 2.1 eV can absorb and utilize a large fraction of visible light up to 600 nm, and Ta_3N_5 nanomaterials[26–29] and/or films[30–35] have been prepared as visible-light-driven (VLD) photocatalysts. Herein, by using Ta_3N_5 as a model semiconductor, we report the design and preparation of Ta_3N_5-Pt nonwoven cloth that is composed of nanofibers constructed from Ta_3N_5 nanoparticles, hierarchical nanopores and Pt nanoparticles. The macroscale Ta_3N_5-Pt nonwoven cloth exhibits large surface area (23.1 m^2 g^{-1}). Furthermore, it can be used as an efficient, stable and easily recyclable macroscale semiconductor photocatalyst with nanostructure, for the degradation of both methylene blue (MB) dye and parachlorophenol (4-CP) under visible light irradiation. This finding promotes the design and development of novel kind of macroscale photocatalysts with nanostructure for practical application, for example, degrading pollutants in lake and/or river.

Results

Synthesis and characterization of the nonwoven cloth. Ta_3N_5-Pt nonwoven cloth was prepared by an electrospinning-calcination-nitridation-wet impregnation method, as demonstrated in Figure 1. First step was to prepare PVP/Ta_2O_5/$Ta(OEt)_4$ composite nonwoven cloth, by electrospinning the solution (ethanol-acetic acid mixture (3.3 : 1, volume ratio) containing 10 wt% tantalum ethanolate ($Ta(OEt)_4$) and 5 wt% polyvinylpyrrolidone (PVP, $M_W \approx$ 1300000 g mol^{-1})) at a high voltage of 15 kV, and followed by the hydrolysis process. The as-prepared PVP/Ta_2O_5/$Ta(OEt)_4$ composite nonwoven cloth is white, and its typical photograph (area: $\sim 10 \times 9.5$ cm^2) is shown in Figure 2a. In fact, in our case, the area of the nonwoven cloth can be easily tuned in a broad range ($10^{-4} \sim 1$ m^2) by changing the collecting region of aluminum foil during the electrospinning process. This macroscopic nonwoven cloth is composed of plenty of individual straight fibers with smooth surface and diameters ranging from 250 to 300 nm, as revealed in scanning electron microscopy (SEM) images (Figures 2b, 2c).

The second step was to calcine the composite nonwoven cloth at 600°C in air for 6 h, for removing polymer component and obtaining inorganic nonwoven cloth based on Ta_2O_5 fibers. After the calcination process, this Ta_2O_5 nonwoven cloth still has the macroscopic morphology (Figure 2d) similar to that (Figure 2a) of the as-prepared PVP/Ta_2O_5/$Ta(OEt)_4$ composite cloth, indicating that the calcination process has no obvious adverse effect on the macroscopic morphology. However, after the calcination, there are obvious changes in the microstructure of the cloth. This Ta_2O_5 nonwoven cloth consists of the pores and bent fibers that interweave and/or stick together (Figures 2e, 2f), which results from the disappearance of PVP component and the high-temperature anneal of Ta_2O_5 component. Furthermore, the diameters of Ta_2O_5 fibers shrink to 200–250 nm, and the fibers with rough surface are composed of nanoparticles with diameter of about 10 nm (Figures 2e, 2f).

The third step was to further nitridize Ta_2O_5 cloth at 800°C under NH_3 flow (500 mL min^{-1}) for 8 h to obtain Ta_3N_5 cloth. It should be noted that Ta_2O_5 nonwoven cloth was tailored to $\sim 4.5 \times 3$ cm^2 to fit the small inter-diameter (~5 cm) of the quartz furnace tube during the nitridation process. Obviously, such Ta_3N_5 cloth is still free-standing and can be easily transferred and/or recycled for further practical application. Its color turned from white to red-orange, as demonstrated vividly in Figure 2g, indicating the conversion from Ta_2O_5 to Ta_3N_5. SEM images (Figures 2h, 2i) reveal that Ta_3N_5 cloth is also composed of hierarchical pores (diameter: 0.2–1 μm) and fibers. The diameters of Ta_3N_5 fibers were reduced to 150–200 nm, and these fibers also interweave and/or stick together. Importantly, Ta_3N_5 fibers are comprised of plenty of nanoparticles with diameters of ~25 nm and nanopores with diameters of ~15 nm (Figure 2i), probably resulting in high surface area. Further information about Ta_3N_5 fibers was obtained from the transmission electron microscopy (TEM) images (Figures 2j–l). The TEM images (Figures 2j–l) confirm that Ta_3N_5 cloth is composed of fibers that are constructed from nanoparticles and nanopores, which agrees well with that revealed by the SEM images. The high-resolution TEM image (Figure 2l) taken from one nanoparticle in the fiber (Figure 2k) shows clear lattice fringes with an interplane spacing of 0.363 nm, which is corresponding to the (110) crystal plane of monoclinic Ta_3N_5. It should be noted that when the nitridation temperature was above 900°C, significant collapse of fibers occurred, resulting in the distortion of Ta_3N_5 cloth (Supplementary Figure S1).

At last, Ta_3N_5 cloth was decorated with Pt nanoparticles (~0.5 wt%) by the photocatalytic reduction of H_2PtCl_6 in methanol aqueous solution under a 300 W xenon lamp light irradiation. The decoration process of Pt has no obvious effects on the shape of cloth, as confirmed by photo (the inset of Figure 2m) and SEM image (Figure 2m). However, from the TEM image (Figure 2n), one can find that there are plenty of nanoparticles with the size of about 2.5 nm on the surface of fibers. The high-resolution TEM image (Figure 2o) shows clear lattice fringes with an interplane spacing of 0.225 nm, which is corresponding to the (111) crystal plane of cubic Pt. Thus, one can confirm the formation of Ta_3N_5-Pt nonwoven cloth with well-defined heterostructure.

The phase and pore structure, and optical characterizations. The phase structure of Ta_3N_5-Pt nonwoven cloth was further investigated.

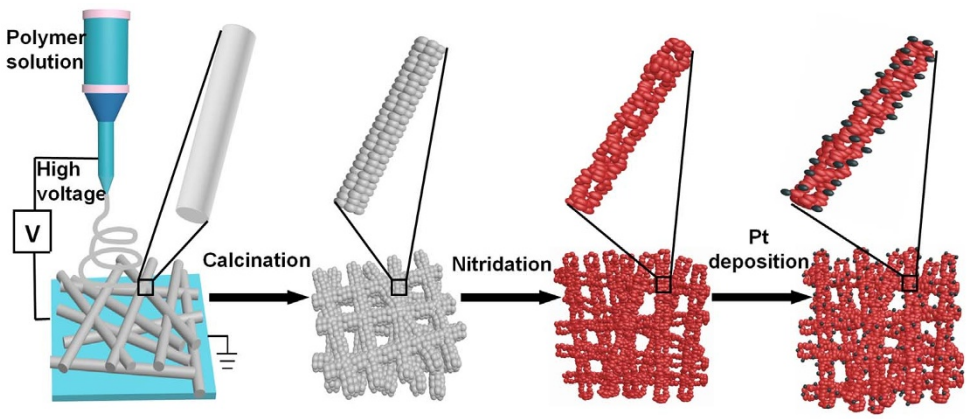

Figure 1 | Schematic illustration of the preparation of Ta_3N_5-Pt nonwoven cloth.

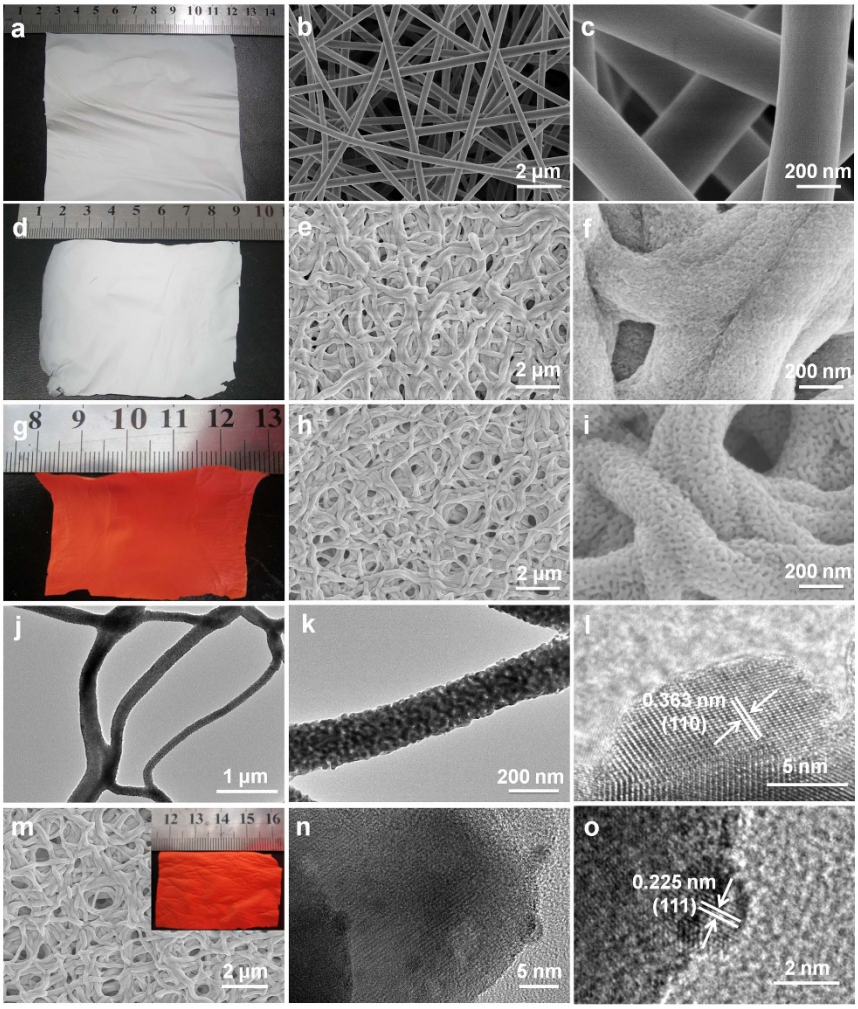

Figure 2 | The photos and microscopy images of samples. (a–c) The photo and SEM images of as-prepared PVP/Ta_2O_5/$Ta(OEt)_4$ composite nonwoven cloth. (d–f) The photos and SEM images of Ta_2O_5 nonwoven cloth after the anneal in air at 600°C for 6 h. (g–i) The photo and SEM images of Ta_3N_5 nonwoven cloth after the nitridation at 800°C under NH_3 flow (500 mL min^{-1}) for 8 h. (j–l) TEM images of nanofibers from Ta_3N_5 nonwoven cloth and HR-TEM image of one nanoparticle in the nanofiber from Ta_3N_5 nonwoven cloth. (m–o) SEM image of Ta_3N_5-Pt nonwoven cloth, TEM image of Ta_3N_5 fiber decorated with Pt nanoparticles and HR-TEM image of one Pt nanoparticle on the surface of the nanofiber from Ta_3N_5-Pt nonwoven cloth.

Figure 3a shows the X-ray diffraction (XRD) patterns of Ta_2O_5, Ta_3N_5 and Ta_3N_5-Pt nonwoven cloths. Obviously, Ta_2O_5 cloth is amorphous, while Ta_3N_5 cloth is well crystallized. All of the diffraction peaks for Ta_3N_5 cloth are characteristic of the monoclinic Ta_3N_5 (JCPDS Card No. 89-5200) (System: monoclinic, System group: C2/m(12), a = 10.229 Å, b = 3.875 Å, c = 10.229 Å). In addition, no characteristic peaks peculiar to the source materials or other impurities are observed. After the decoration of Pt nanoparticles, the XRD pattern of the Ta_3N_5-Pt cloth is quite similar to that of the Ta_3N_5 cloth. No obvious diffraction peaks from Pt can be detected, which should be attributed to the low amount of Pt on the Ta_3N_5-Pt cloth.

Subsequently, the nitrogen adsorption/desorption isotherms of Ta_3N_5 cloth and Ta_3N_5-Pt cloth were investigated (Figure 3b). The Brunauer–Emmett–Teller (BET) surface area of Ta_3N_5 cloth is calculated to be 22.0 m^2 g^{-1}. After the deposition of Pt nanoparticles, Ta_3N_5-Pt cloth exhibits a slight increase of BET surface area (23.1 m^2 g^{-1}). Thus, although both Ta_3N_5 cloth and Ta_3N_5-Pt cloth are macroscale, they have high surface area compared with those of bulk powders (Figure S4) and traditional fibers, resulting from their nanostructure. Moreover, the pore size distributions, which are calculated from the desorption branches, reveal the existence of nanopores in both Ta_3N_5 cloth and Ta_3N_5-Pt cloth (the inset of Figure 3b). The nanopores in Ta_3N_5 cloth have the diameter of about 15 nm, while those in Ta_3N_5-Pt cloth have the diameter of about 13 nm, which agrees with that revealed by the SEM and TEM images (Figures 2h–k, 2m). The presence of nanopores in fibers and macro-pores among fibers may greatly improve the physicochemical properties and/or serve as transport paths for small molecules.

The optical properties of Ta_2O_5, Ta_3N_5 and Ta_3N_5-Pt cloths were studied by using an UV-Vis-NIR spectrometer (Figure 3c). The spectrum of Ta_2O_5 cloth is similar to what has been reported previously for Ta_2O_5 samples[26], and it exhibits a short-wavelength absorption edge at approximately 330 nm. Importantly, Ta_3N_5 cloth shows a large red shift from 330 to 600 nm, due to the band gap narrowing caused by the substitution of N for O atoms[36], which agrees well with the reported value for the bandgap ($Eg \approx 2.1$ eV) of Ta_3N_5 samples[26,30]. Furthermore, after the decoration of Pt, no obvious change of absorption spectrum has been observed. These facts indicate that both Ta_3N_5 cloth and Ta_3N_5-Pt cloth have a broad region of visible-light photo-response, and therefore can be expected to act as excellent VLD photocatalysts.

Photocatalytic activity. In order to investigate the potential of Ta_3N_5-Pt cloth as VLD photocatalyst, the photocatalytic activity of macroscopic Ta_3N_5-Pt cloth was evaluated by immersing the cloth in

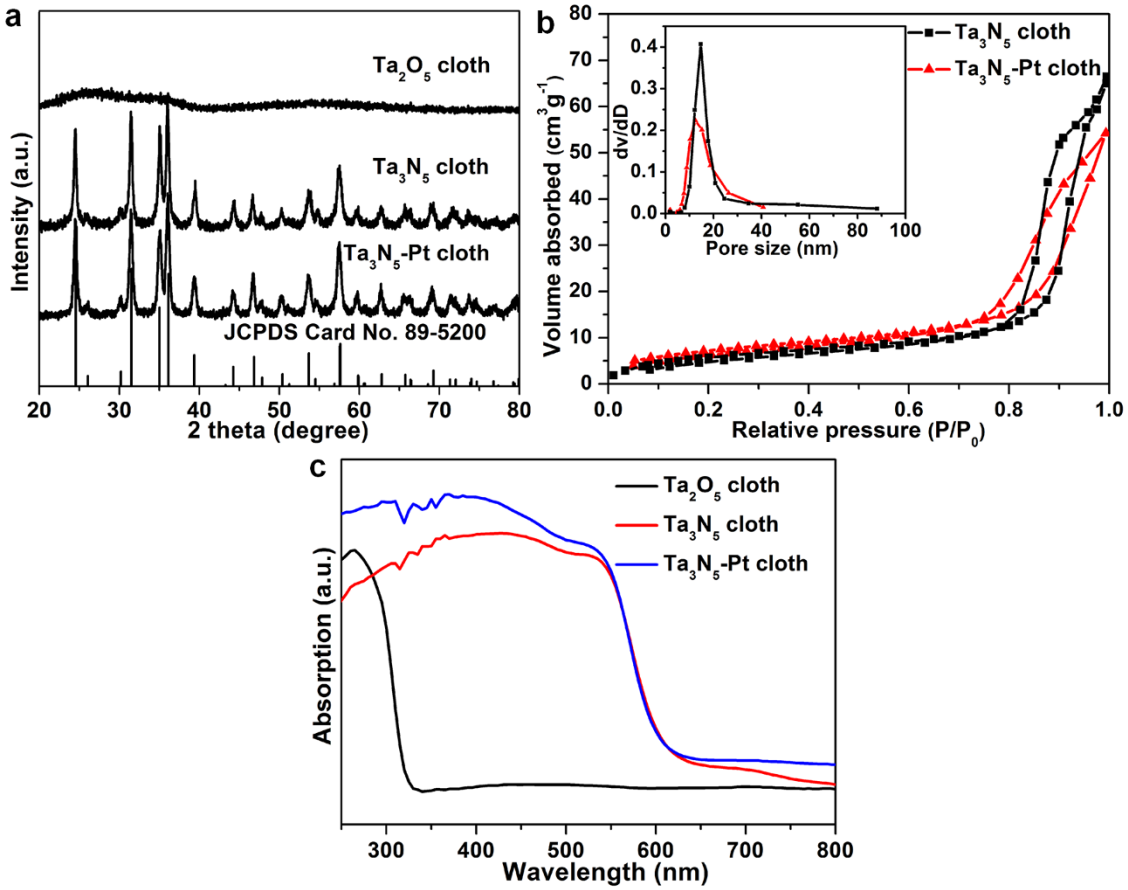

Figure 3 | The phase and pore structure, and optical characterizations. (a) The X-ray diffraction (XRD) patterns of Ta_2O_5 nonwoven cloth, Ta_3N_5 nonwoven cloth, Ta_3N_5-Pt nonwoven cloth and standard XRD pattern of Ta_3N_5 (JCPDS No. 89-5200). (b) Nitrogen adsorption–desorption isotherms of the Ta_3N_5 cloth and Ta_3N_5-Pt cloth. (c) The ultraviolet–visible diffuse reflectance spectra of Ta_2O_5 cloth, Ta_3N_5 cloth and Ta_3N_5-Pt cloth.

the solution containing MB dye or colorless 4-CP as the model pollutant (Figure 4). For comparison, bulk Ta_3N_5 powder, bulk Ta_3N_5 powder decorated with Pt nanoparticles (denoted as bulk Ta_3N_5-Pt powder), and mesoporous SiO_2 powder decorated with Pt nanoparticles (denoted as SiO_2-Pt powder) were also prepared and used as the photocatalysts. These bulk powders were also characterized by XRD, SEM, BET, UV-Vis-NIR spectrometer or TEM (Supplementary Figures S2–S6).

When MB dye was used as the model of organic pollutant, the photocatalytic activity of macroscopic Ta_3N_5-Pt cloth was evaluated by immersing the cloth (20 mg, size: ~2.5 × 3.5 cm^2) in 60 mL aqueous solution containing 10 mg L^{-1} methylene blue (MB) dye under visible light irradiation ($\lambda > 400$ nm). When dissolved in distilled water, MB dye displays a major absorption band centered at 663 nm, which is used to monitor the photocatalytic degradation. With the macroscopic Ta_3N_5–Pt cloth as the photocatalyst, the temporal evolution of the absorption spectra of MB is shown in Supplementary Fig. S7. A rapid decrease of MB absorption at wavelength of 663 nm is observed, accompanied with an absorption band shift to shorter wavelengths. The color of MB solution gradually changes from initially blue to transparent as the reaction proceeds (the inset of Fig. S7), indicating that Ta_3N_5–Pt cloth exhibits excellent photocatalytic activity for the degradation of MB. For comparison, the photodegradation of MB without photocatalyst (blank test) and with SiO_2-Pt, bulk Ta_3N_5 powder, bulk Ta_3N_5-Pt powder, or Ta_3N_5 cloth, was also measured under the other identical conditions, respectively (Figure 5a). The blank test indicates that the degradation of MB is extremely slow without photocatalyst under visible light illumination. By using bulk Ta_3N_5 powder as the VLD photocatalyst, the photodegradation efficiency of MB can just approach 59.8% after 60 min of reaction. When using Ta_3N_5 cloth as the photocatalyst, 79.4% of MB is photocatalytically degraded after 60 min. This indicates that Ta_3N_5 cloth exhibits higher photocatalytic activity than bulk Ta_3N_5 powder, which can be attributed to its higher BET surface area and hierarchical nanopores. Interestingly, after the decoration with Pt nanoparticles, the Ta_3N_5–Pt cloth can degrade 97.2% of MB after 60 min, indicating the highest photocatalytic activity. To investigate the role of Pt nanoparticles in the photocatalytic process,

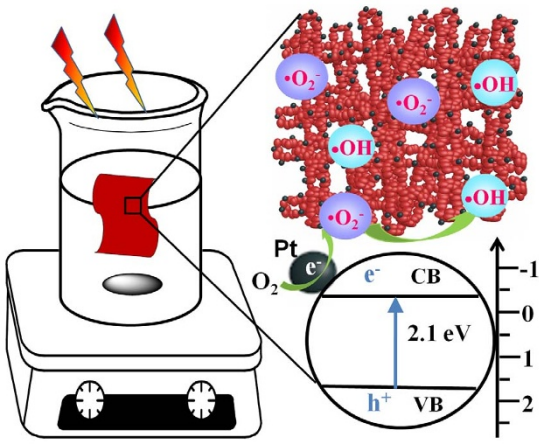

Figure 4 | Schematic illustration of experimental setups and photocatalytic process.

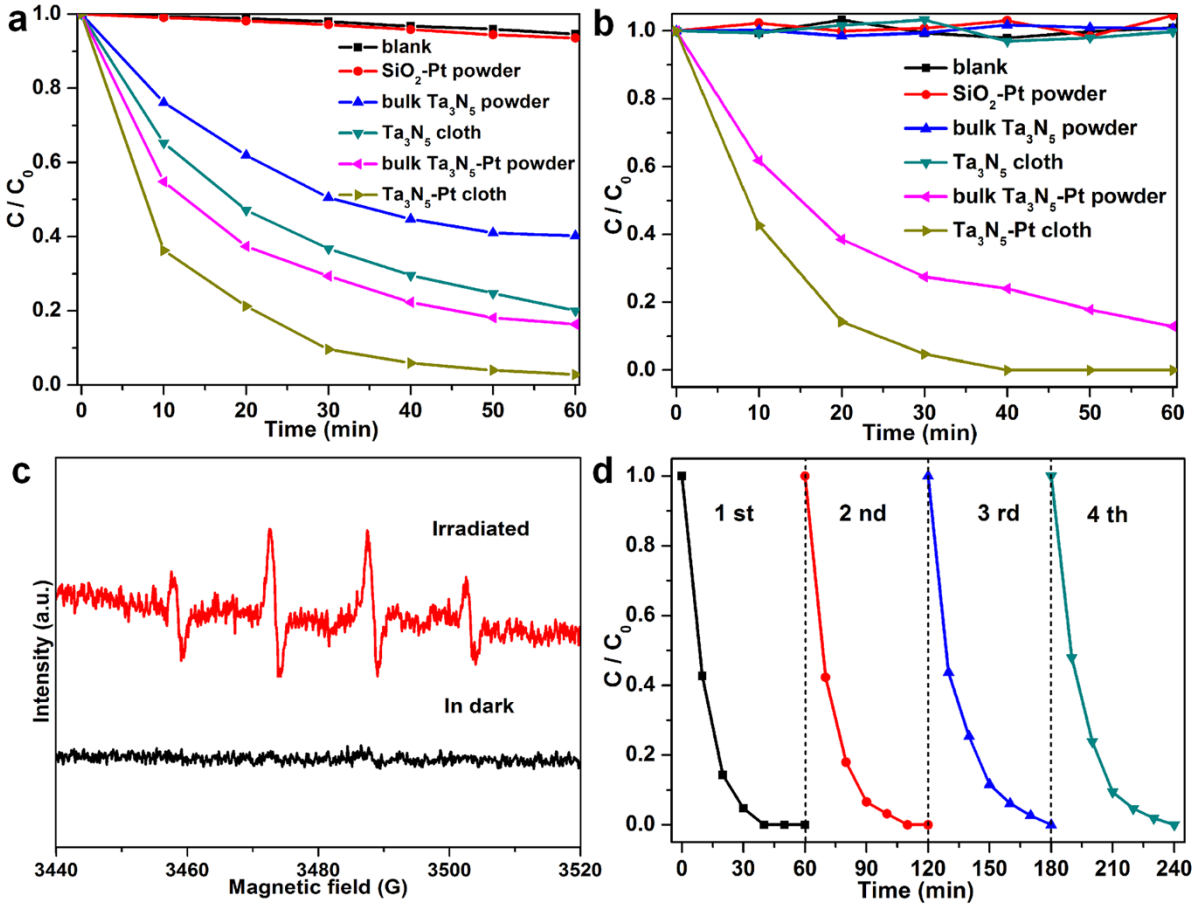

Figure 5 | Photocatalytic performances of Ta_3N_5-Pt cloth. The degradation efficiency of (a) MB aqueous solution (10 mg L^{-1}, 60 mL) and (b) 4-CP aqueous solution (1.28 mg L^{-1}, 60 mL), versus the exposure time under visible light irradiation ($\lambda > 400$ nm), in the absence of photocatalyst and in the presence of SiO_2–Pt powder, bulk Ta_3N_5 powder, bulk Ta_3N_5-Pt powder, Ta_3N_5 cloth or Ta_3N_5-Pt cloth. (c) DMPO spin-trapping ESR spectra recorded at ambient temperature in the aqueous solution with Ta_3N_5 cloth for DMPO-·OH under visible light irradiation ($\lambda = 532$ nm). (d) Cycling photocatalytic test of Ta_3N_5–Pt nonwoven cloth (20 mg).

the photocatalytic degradation of MB was conducted in the presence of SiO_2-Pt powder and bulk Ta_3N_5-Pt powder, respectively. Obviously, the SiO_2-Pt is inactive under visible light irradiation, and the photodegradation of MB is even similar to that of the blank test, which reveals that both SiO_2 and Pt have no photocatalytic activity. However, after the deposition of Pt, bulk Ta_3N_5-Pt powder exhibits the improved photodegradation efficiency (83.7%) of MB after 60 min, compared with that (59.8%) of bulk Ta_3N_5 powder. These facts indicate that Pt nanoparticles can greatly improve the photocatalytic activities of Ta_3N_5, which results from the fact that Pt act as electron trap to facilitate the separation of photogenerated electron-hole pairs and promote interfacial electron transfer process[37,38].

When colorless parachlorophenol (4-CP) was used as the model of organic pollutant, the photocatalytic activity of macroscopic Ta_3N_5-Pt cloth was evaluated by immersing the cloth (20 mg, size: ~2.5 × 3.5 cm^2) in 60 mL aqueous solution containing 1.28 mg L^{-1} 4-CP under visible light irradiation ($\lambda > 400$ nm). 4-CP as a typical pollutant has no photolysis and no visible light absorption characteristics in the photodegradation process. When the macroscopic Ta_3N_5–Pt cloth was used as the photocatalyst, the temporal degradation of 4-CP was determined by high-performance liquid chromatography (HPLC) profiles (Supplementary Fig. S8). The peak with retention time of 8.5 min is attributed to the initial 4-CP and is used to monitor the photocatalytic degradation. As the reaction proceeds, the peak decreases rapidly in the reaction, indicating that Ta_3N_5–Pt cloth exhibits high photocatalytic activity for the degradation of 4-CP. For comparison, the photodegradation of 4-CP without photocatalyst and with SiO_2-Pt, bulk Ta_3N_5 powder, Ta_3N_5 cloth or bulk Ta_3N_5-Pt powder, was also measured with otherwise identical conditions, respectively (Figure 5b). The photodegradation of 4-CP without photocatalyst and with SiO_2-Pt, bulk Ta_3N_5 powder or Ta_3N_5 cloth is extremely slow and nearly no 4-CP is degraded after 60 min. Surprisingly, after decoration with Pt nanoparticles, the photocatalytic performances of both bulk Ta_3N_5-Pt powder and Ta_3N_5-Pt cloth are dramatically improved for the degradation of 4-CP. After 60 min of visible light irradiation, the Ta_3N_5–Pt powder exhibits higher photodegradation efficiency of 4-CP (87.2%) than that by Ta_3N_5 cloth, which can be attributed to the enhanced separation of photogenerated electron-hole pairs in Ta_3N_5-Pt heterostructure. With macroscopic Ta_3N_5-Pt cloth as photocatalyst, only a 40 min period was required to decompose all the 4-CP in the solution (Supplementary Fig. S8 and Fig. 5b), further demonstrating the highest photocatalytic activity. Compared with bulk Ta_3N_5-Pt powder, the outstanding photocatalytic activity for the degradation of 4-CP by Ta_3N_5-Pt cloth can be ascribed to its relatively higher BET surface area (23.1 m^2 g^{-1}) and special hierarchical structure.

It is well known that mineralization is the ultimate goal in pollutant treatment. Total organic carbon (TOC) value as an important index for the mineralization of organic species, was studied in the photodegradation of 4-CP (60 mL, 20 mg L^{-1}) by 250 mg of Ta_3N_5-Pt cloth (Supplementary Fig. S9). It is clear that the TOC concentration of the solution continuously decreases, indicating that 4-CP is steadily mineralized by Ta_3N_5-Pt cloth photocatalyst under visible

light irradiation. After 120 min of irradiation, the TOC concentration decreases from 10.76 mg L^{-1} to 3.66 mg L^{-1}, reaching a high mineralization ratio of 66%. This fact demonstrates that Ta_3N_5-Pt cloth can efficiently degrade and mineralize organic pollutants under the irradiation of visible light.

It has been reported that the conduction and valence band edges of Ta_3N_5 at pH 0, are at approximately −0.4 V and +1.7 V versus NHE, respectively[39]. Since the redox potential value of photogenerated hole ($\varphi(h^+)$) is approximately equal to that (+1.7 V) of the valance band, the $\varphi(h^+)$ is lower than $\varphi(OH\bullet/H_2O)$(+2.38 V versus NHE)[14]. As a result, the •OH radicals can not be produced via the direct oxidation of H_2O molecules by photo-induced holes. The photogenerated electron ($\varphi(e^-)$) is more negative than $\varphi(O_2/\bullet O_2^-)$(−0.33 V versus NHE), which allows the production of $\bullet O_2^-$ via the reduction of O_2 by conduction band electrons. To confirm this conjecture, the electron spin resonance (ESR) technique (with 5,5-dimethyl-pyrroline N-oxide, DMPO) was used to obtain the information on the active radicals involved in the solution with Ta_3N_5 cloth irradiated by visible light or un-irradiated. Because $\bullet O_2^-$ in water is very unstable and undergoes facile disproportionation rather than slow reaction with DMPO[40], the involvement of $\bullet O_2^-$ was examined in DMSO in which the DMPO-$\bullet O_2^-$ has a longer life time[41]. The characteristic peaks of the DMPO-$\bullet O_2^-$ adducts were observed in DMSO solution with Ta_3N_5 cloth irradiated by visible light (Supplementary Fig. S10), while no $\bullet O_2^-$ signal was detected in dark under otherwise identical conditions, which are in good agreement with the previous report[42]. Recently, there are several reports revealed that the •OH can be generated from $\bullet O_2^-$ with the assistance of the photoinduced electrons[43–45]. In our case, to confirm the presence of •OH in the photocatalytic process, the aqueous solution with Ta_3N_5 cloth irradiated by visible light or in dark was measured by ESR. As shown in Figure 5c, the four characteristic peaks of DMPO-•OH (1 : 2 : 2 : 1 quartet pattern) were also observed in aqueous solution with Ta_3N_5 cloth irradiated with visible light, while no •OH signal was detected in dark under otherwise identical conditions. This fact demonstrates that the •OH can be produced from $\bullet O_2^-$, which is similar to the previous reports[43–45]. These ESR results confirm that •OH and $\bullet O_2^-$ were produced in the solution with Ta_3N_5 cloth under the irradiation of visible light, and they are supposed to finally induce the decomposition of organic pollutants.

Most importantly, the macroscopic Ta_3N_5-Pt cloth (present area: ~4.5 × 2.6 cm^2) can be easily transferred and/or recycled in photocatalytic application. To evaluate the stability and reusability of macroscopic Ta_3N_5-Pt cloth, a recycling test was performed, as shown in Figure 5d. The photodegradation of 4-CP was monitored for four cycles (each cycle lasted 60 min). After each cycle, the macroscopic Ta_3N_5-Pt cloth was taken out and washed with water. Then the cloth was immersed in the same volume (60 mL) of fresh 4-CP solution again. The photocatalytic activity of Ta_3N_5-Pt cloth does not significantly decrease in the cycling test and the photodegradation efficiency of 4-CP can still reach 100% for the fourth cycle. Thus, during four cycles, there is no significant loss of photocatalytic activity. The SEM image and the XRD patterns (Supplementary Fig. S11) further confirm that there are no obvious changes in the morphology and the crystalline phase of Ta_3N_5-Pt cloth before and after recycling reactions, indicating excellent stability and reusability of Ta_3N_5-Pt cloth.

Discussion

On the basis of the above results and energy band diagram, the photocatalytic process of Ta_3N_5-Pt cloth can be proposed, as shown in Figure 4. The photocatalytic activity of macroscopic Ta_3N_5-Pt cloth was evaluated by immersing the cloth in aqueous solution containing model pollutant due to its macroscale size (present area: ~4.5 × 2.6 cm^2). Ta_3N_5 with the narrow band-gap (2.1 eV) has a broad range of visible-light photo-response and can exhibit efficient visible-light photoabsorption. The photocatalytic reaction is initiated by the absorption of visible-light photons with energy equal or higher than the band-gap in Ta_3N_5 semiconductor, which results in the creation of photogenerated holes in its valence band (VB) and electrons in its conduction band (CB). Because of the small particle size of Ta_3N_5 nanoparticles (~25 nm), the charge carriers can quickly travel to the surface of the catalyst from the interior. Then CB-electrons easily flow into metal Pt through the Schottky barrier because the CB (or the Fermi level) of Ta_3N_5 is higher than that of the loaded metal Pt, which is consistent with the previous study on electron transfer from semiconductor (such as TiO_2) to Pt[37,38]. This process of fast electron transfer contributes to enhancing interfacial charge transfer and realizing the efficient separation of VB-holes and CB-electrons in the heterostructures[37,38]. Thus, plenty of CB-electrons in Pt component are available to reduce O_2 to produce $\bullet O_2^-$, which can be further transformed into •OH with the assistance of the photo-induced electrons[43–45]. Under successive attacks by $\bullet O_2^-$ and •OH, MB and 4-CP were effectively photodegraded, as demonstrated in Figures 5a,b and Supplementary Figures S7–S9.

It is noteworthy that hierarchical pores in Ta_3N_5-Pt cloth are supposed to play an important role in this photocatalytic process. As mentioned above, there are plenty of nanopores with diameter of ~13 nm inside Ta_3N_5-Pt fibers and micro-pores with sizes of 0.2–1 μm beside Ta_3N_5 fibers, probably resulting in two positive effects. The one effect is that micro-pores with sizes of 0.2–1 μm increase the photoscattering and absorption of visible light (Supplementary Fig. S12), since the photoabsorption can be enhanced if the nanoarrays are aligned with photonic-crystal microstructures, and/or the faceted end planes of well-shaped crystals serve as good laser-cavity mirrors[46,47] The other results from the fact that the hierarchical combination of smaller nanopores and larger macro-pores can be considered as transport paths[48]. It has been reported that chemical reactions can occur more easily when the transport paths, through which reactant molecules move in or out of the nanostructured materials, are included as an integral part of the architectural design[49]. The textural transport paths have been revealed to have the beneficial effect on photocatalysis[48,50]. We believe that the presence of transport paths in Ta_3N_5-Pt cloth also benefits the pollutant molecules to get to the reactive sites on the framework walls of photocatalysts, which results in excellent photocatalytic activity. Furthermore, these transport paths as well as macroscale size probably make Ta_3N_5-Pt cloth used as "microfiltration membrane" with photocatalytic activity, probably resulting in a very promising application as "photocatalyst dam" for the polluted river in the future (Supplementary Fig. S13).

In summary, macroscopic Ta_3N_5-Pt nonwoven cloth with hierarchical nanopores has been synthesized by an electrospinning-calcination-nitridation-wet impregnation method. Such free-standing cloth is composed of nanofibers constructed from Ta_3N_5 nanoparticles, hierarchical nanopores and Pt nanoparticles. Under visible light illumination, it exhibits excellent photocatalytic activities on MB and 4-CP degradation. Furthermore, it can be easily transferred and/or recycled, with good stability. It should be noted that the present Ta_3N_5-Pt cloth is still relatively fragile, further work should be carried out for obtaining Ta_3N_5-Pt cloth with better strength and flexibility, and work in this direction is already ongoing. More importantly, this work provides some insight into the design and development of novel, efficient and easily recyclable macroscale photocatalysts with nanostructure, for future practical photocatalytic application, for example, as "photocatalyst dam" for the photodegradation of organic pollutants in the polluted river.

Methods

Materials synthesis. *Synthesis of Ta_3N_5 nonwoven cloth.* At first, 10 wt% $Ta(OEt)_4$ was dissolved in an ethanol-acetic acid mixture (3.3 : 1, volume ratio). Then, 5 wt%

polyvinylpyrrolidone (PVP, $M_W \approx 1300000$ g mol^{-1}) was added to the above solution. After vigorously stirring for 24 h, the precursor solution was loaded into a plastic syringe and the feeding rate was kept constant at 0.3 ml h^{-1} using a syringe pump. A high voltage of 15 kV was applied between the orifice and grounded aluminum foil at a distance of 20 cm. The collected PVP/Ta_2O_5/$Ta(OEt)_4$ composite cloth was calcined at 600°C in air for 6 h to obtain Ta_2O_5 nonwoven cloth. The Ta_2O_5 cloth was further nitridized at 800°C under an ammonia flow (500 mL min^{-1}) for 8 h to obtain Ta_3N_5 nonwoven cloth.

Synthesis of Ta_3N_5-Pt nonwoven cloth. Pt (0.5 wt%) was loaded on Ta_3N_5 nonwoven cloth by the photocatalytic reduction of H_2PtCl_6 in methanol aqueous solution under a 300 W xenon lamp light irradiation for 4 h.

Mesoporous SiO_2 was prepared according to the reference[51]. SiO_2-Pt powder: Pt (0.5 wt%) was loaded on SiO_2 by the photocatalytic reduction of H_2PtCl_6 in methanol aqueous solution under a 300 W xenon lamp light irradiation for 4 h.

Bulk Ta_3N_5 powder was prepared by thermal nitridation of bulk Ta_2O_5 powder synthesized in our laboratory. Bulk Ta_2O_5 powder: 2.5 g $Ta(OEt)_4$ was dissolved in 30 ml absolute alcohol to obtain $Ta(OEt)_4$ solution, then the ethanolic $Ta(OEt)_4$ solution was quickly added into 30 ml aqueous solution with pH8 under magnetic stirring, the precipitate was collected by centrifugation, washed with ethanol and distilled water, and dried in an oven at 100°C, then the dried precipitate was calcined at 800°C for 3 h; Bulk Ta_3N_5 powder: Bulk Ta_2O_5 powder was nitridized at 850°C under an ammonia flow (500 mL min^{-1}) for 15 h to obtain bulk Ta_3N_5 powder.

Bulk Ta_3N_5-Pt powder. The procedure of Pt loading is the same as that of Ta_3N_5-Pt nonwoven cloth except that the Ta_3N_5 nonwoven cloth was replaced by bulk Ta_3N_5 powder.

Characterizations. X-ray diffraction (XRD) measurements were recorded on a D/max-2550 PC X-ray diffractometer using Cu Kα radiation ($\lambda = 0.15418$ nm). The scanning electron microscope (SEM) characterizations were performed on a Hitachi S-4800 field emission scanning electron microscope. The transmission electron microscope (TEM) analyses were performed by a JEOL JEM-2010F high-resolution transmission electron microscope. The optical diffuse reflectance spectrum were conducted on a UV-VIS-NIR scanning spectrophotometer (UV-3101PC, Shimadzu) using an integrating sphere accessory. Nitrogen absorption–desorption measurement were conducted on a Micromeritics ASAP 2020 nitrogen adsorption apparatus (USA). The BET surface area was determined by a multipoint BET method using the adsorption data in the relative pressure (P/P_0) range of 0.05–0.3. A desorption isotherm was used to determine the pore size distribution via the Barret–Joyner–Halender (BJH) method, assuming a cylindrical pore model. Electron paramagnetic resonance (EPR) signals of paramagnetic species spin-trapped with 5,5-dimethyl-pyrroline N-oxide (DMPO) were recorded with a Bruker ESR 300E spectrometer. The irradiation source was a Quanta-Ray Nd:YAG pulsed laser system ($\lambda = 532$ nm, 10 Hz). The total organic carbon (TOC) values were detected by a Shimadzu TOC-VCPH total organic carbon analyzer.

Photocatalytic tests. Photocatalytic activities of the photocatalysts were evaluated by degradation of Methylene Blue (MB) dye and parachlorophenol (4-CP) contaminant in an aqueous solution under visible light irradiation using a 300 W xenon lamp (Beijing Perfect Light Co. Ltd., Beijing) with a cut-off filter ($\lambda > 400$ nm) as light source. In each experiment, Ta_3N_5 cloth (20 mg, size: ~2.5 × 3.5 cm^2), Ta_3N_5-Pt cloth (20 mg, size: ~2.5 × 3.5 cm^2), mesoporous SiO_2-Pt (20 mg), bulk Ta_3N_5 powder (20 mg) or bulk Ta_3N_5-Pt powder (20 mg) as photocatalyst was added into 60 mL of MB aqueous solution (10 mg L^{-1}) and 60 mL of parachlorophenol aqueous solution (1.28 mg L^{-1}). The temperature of the reaction solution was controlled at 22 ± 2°C by cooling water. Before illumination, the suspension was mildly magnetically stirred in the dark for 3 h to ensure that an adsorption/desorption equilibrium was established between the photocatalysts and the target contaminant (MB and 4-CP). When the remaining MB and 4-CP concentration needed to be measured, at given irradiation time intervals (10 min), 3 mL aliquots were collected and centrifuged to remove the remaining solids for analysis. Then, for the photocatalytic test of MB, the absorption UV-vis spectra of the solution were recorded on a U-2910 UV-vis spectrophotometer (Hitachi, Japan). For the photocatalytic test of 4-CP, the 4-CP concentrations in the solutions were analyzed by high-performance liquid chromatography (HPLC) using an Agilent 1100 series (USA) equipped with a diode array detector (DAD) with wavelength set at 280 nm directly after filtration through a 0.22 μm hydrofacies syringe filter. The mobile phase was methanol (80%) and water (20%) and the flow rate was 0.5 mL min^{-1}; In the TOC test, 250 mg of Ta_3N_5-Pt cloth was added into 60 mL of parachlorophenol aqueous solution (20 mg L^{-1}). In the stability and reusability test of the catalyst, four consecutive cycles were tested. The catalysts were washed thoroughly with water and dried after each cycle, and then the cloth was immersed in the same volume (60 mL) of fresh parachlorophenol aqueous solution (1.28 mg L^{-1}) again.

1. Hoffmann, M. R., Martin, S. T., Choi, W. & Bahnemann, D. W. Environmental applications of semiconductor photocatalysis. *Chem. Rev.* **95**, 69–96 (1995).
2. Asahi, R., Morikawa, T., Ohwaki, T., Aoki, K. & Taga, Y. Visible-light photocatalysis in nitrogen-doped titanium oxides. *Science* **293**, 269–271 (2001).
3. Kubacka, A., Fernández-García, M. & Colón, G. Advanced nanoarchitectures for solar photocatalytic applications. *Chem. Rev.* **112**, 1555–1614 (2012).
4. Chen, X., Liu, L., Yu, P. Y. & Mao, S. S. Increasing solar absorption for photocatalysis with black hydrogenated titanium dioxide nanocrystals. *Science* **331**, 746–750 (2011).
5. Roy, P., Berger, S. & Schmuki, P. TiO_2 nanotubes: synthesis and applications. *Angew. Chem. Int. Ed.* **50**, 2904–2939 (2011).
6. Wu, H. B., Hng, H. H. & Lou, X. W. Direct synthesis of anatase TiO_2 nanowires with enhanced photocatalytic activity. *Adv. Mater.* **24**, 2567–2571 (2012).
7. Liu, G. *et al.* Visible light responsive nitrogen doped anatase TiO_2 sheets with dominant {001} facets derived from TiN. *J. Am. Chem. Soc.* **131**, 12868–12869 (2009).
8. Sun, J. H. *et al.* Bioinspired hollow semiconductor nanospheres as photosynthetic nanoparticles. *Nat. Commun.* **3**, 1139 (2012).
9. Xiong, Z. & Zhao, X. S. Nitrogen-doped titanate-anatase core–shell nanobelts with exposed {101} anatase facets and enhanced visible light photocatalytic activity. *J. Am. Chem. Soc.* **134**, 5754–5757 (2012).
10. Li, R. G. *et al.* Spatial separation of photogenerated electrons and holes among {010} and {110} crystal facets of $BiVO_4$. *Nat. Commun.* **4**, 1432 (2013).
11. Xi, G. *et al.* In situ growth of metal particles on 3D urchin-like WO_3 nanostructures. *J. Am. Chem. Soc.* **134**, 6508–6511 (2012).
12. Zhang, L. S., Wang, W. Z., Zhou, L. & Xu, H. L. Bi_2WO_6 nano- and microstructures: shape control and associated visible-light-driven photocatalytic activities. *Small* **3**, 1618–1625 (2007).
13. Zhang, L. S. *et al.* Fabrication of flower-like Bi_2WO_6 superstructures as high performance visible-light driven photocatalysts. *J. Mater. Chem.* **17**, 2526–2532 (2007).
14. Zhang, L. S. *et al.* Effective photocatalytic disinfection of *E. coli* K-12 using AgBr-Ag-Bi_2WO_6 nanojunction system irradiated by visible light: the role of diffusing hydroxyl radicals. *Environ. Sci. Technol.* **44**, 1392–1398 (2010).
15. Jiang, D. L., Zhang, S. Q. & Zhao, H. J. Photocatalytic degradation characteristics of different organic compounds at TiO_2 nanoporous film electrodes with mixed anatase/rutile phases. *Environ. Sci. Technol.* **41**, 303–308 (2007).
16. Zhang, L. W., Wang, Y. J., Cheng, H. Y., Yao, W. Q. & Zhu, Y. F. Synthesis of porous Bi_2WO_6 thin films as efficient visible-light-active photocatalysts. *Adv. Mater.* **21**, 1286–1290 (2009).
17. Kitano, M. *et al.* Synthesis of nanowire TiO_2 thin films by hydrothermal treatment and their photoelectrochemical properties. *Catal. Lett.* **119**, 217–221 (2007).
18. Zhang, Z. H., Zhang, L. B., Hedhili, M. N., Zhang, H. N. & Wang, P. Plasmonic gold nanocrystals coupled with photonic crystal seamlessly on TiO_2 nanotube photoelectrodes for efficient visible light photoelectrochemical water splitting. *Nano Lett.* **13**, 14–20 (2013).
19. Agarwal, S., Wendorff, J. H. & Greiner, A. Progress in the field of electrospinning for tissue engineering applications. *Adv. Mater.* **21**, 3343–3351 (2009).
20. Bognitzki, M. *et al.* Nanostructured fibers via electrospinning. *Adv. Mater.* **13**, 70–72 (2001).
21. Jo, E. *et al.* Core-sheath nanofibers containing colloidal arrays in the core for programmable multi-agent delivery. *Adv. Mater.* **21**, 968–972 (2009).
22. Li, D. & Xia, Y. N. Fabrication of titania nanofibers by electrospinning. *Nano Lett.* **3**, 555–560 (2003).
23. Hou, D. F., Luo, W., Huang, Y. H., Yu, J. C. & Hu, X. L. Synthesis of porous $Bi_4Ti_3O_{12}$ nanofibers by electrospinning and their enhanced visible-light-driven photocatalytic properties. *Nanoscale* **5**, 2028–2035 (2013).
24. Liu, Z. Y., Sun, D. D., Guo, P. & Leckie, J. O. An efficient bicomponent TiO_2/SnO_2 nanofiber photocatalyst fabricated by electrospinning with a side-by-side dual spinneret method. *Nano Lett.* **7**, 1081–1085 (2007).
25. Wu, H. *et al.* GaN nanofibers based on electrospinning: facile synthesis, controlled assembly, precise doping, and application as high performance UV photodetector. *Adv. Mater.* **21**, 227–231 (2009).
26. Hara, M. *et al.* TaON and Ta_3N_5 as new visible light driven photocatalysts. *Catal. Today* **78**, 555–560 (2003).
27. Ma, S. S. K., Hisatomi, T., Maeda, K., Moriya, Y. & Domen, K. Enhanced water oxidation on Ta_3N_5 photocatalysts by modification with alkaline metal salts. *J. Am. Chem. Soc.* **134**, 19993–19996 (2012).
28. Wang, D. *et al.* Core/shell photocatalyst with spatially separated co-catalysts for efficient reduction and oxidation of water. *Angew. Chem. Int. Ed.* **52**, 11252–11256 (2013).
29. Wu, C. H. *et al.* Ta_3N_5 nanowire bundles as visible-light-responsive photoanodes. *Chemistry - An Asian Journal* **8**, 2354–2357 (2013).
30. Feng, X. J. *et al.* Ta_3N_5 nanotube arrays for visible light water photoelectrolysis. *Nano Lett.* **10**, 948–952 (2010).
31. Higashi, M., Domen, K. & Abe, R. Fabrication of efficient TaON and Ta_3N_5 photoanodes for water splitting under visible light irradiation. *Energy Environ. Sci.* **4**, 4138–4147 (2011).
32. Kado, Y. *et al.* Enhanced water splitting activity of M-doped Ta_3N_5 (M = Na, K, Rb, Cs). *Chem. Commun.* **48**, 8685 (2012).
33. Zhen, C., Wang, L. Z., Liu, G., Lu, G. Q. & Cheng, H.-M. Template-free synthesis of Ta_3N_5 nanorod arrays for efficient photoelectrochemical water splitting. *Chem. Commun.* **49**, 3019–3021 (2013).
34. Hou, J. G., Yang, C., Wang, Z., Jiao, S. Q. & Zhu, H. M. Cobalt-bilayer catalysts decorated Ta_3N_5 nanorod array as integrated electrodes for photoelectrochemical water oxidation. *Energy Environ. Sci.* **6**, 3322–3330 (2013).

35. Li, Y. *et al.* Cobalt phosphate-modified barium-doped tantalum nitride nanorod photoanode with 1.5% solar energy conversion efficiency. *Nat. Commun.* **4**, 2566 (2013).
36. Fang, C. M. *et al.* The electronic structure of tantalum (oxy)nitrides TaON and Ta_3N_5. *J. Mater. Chem.* **11**, 1248–1252 (2001).
37. Linsebigler, A. L., Lu, G. Q. & Yates, J. T. Photocatalysis on TiO_2 surfaces: principles, mechanisms, and selected results. *Chem. Rev.* **95**, 735–758 (1995).
38. Wang, W.-N. *et al.* Size and structure matter: enhanced CO_2 photoreduction efficiency by size-resolved ultrafine Pt nanoparticles on TiO_2 single crystals. *J. Am. Chem. Soc.* **134**, 11276–11281 (2012).
39. Chun, W.-J. *et al.* Conduction and valence band positions of Ta_2O_5, TaON, and Ta_3N_5 by UPS and electrochemical methods. *J. Phys. Chem. B* **107**, 1798–1803 (2003).
40. Ma, W. H. *et al.* An efficient approach for the photodegradation of organic pollutants by immobilized iron ions at neutral pHs. *Chem. Commun.* 1582–1584 (2003).
41. Ben-Hur, E., Carmichael, A., Riesz, P. & Rosenthal, I. Photochemical generation of superoxide radical and the cytotoxicity of phthalocyanines. *Int. J. Radiat. Biol.* **48**, 837–846 (1985).
42. Lhachatryan, L., Vejerano, E., Lomnicki, S. & Dellinger, B. Environmentally persistent free radicals (EPFRs). 1. generation of reactive oxygen species in aqueous solutions. *Environ. Sci. Technol.* **45**, 8559–8566 (2011).
43. Legrini, O., Oliveros, E. & Braun, A. M. Photochemical processes for water treatment. *Chem. Rev.* **93**, 671–698 (1993).
44. Fujishima, A., Zhang, X. & Tryk, D. TiO_2 photocatalysis and related surface phenomena. *Surf. Sci. Rep.* **63**, 515–582 (2008).
45. Sun, S. *et al.* Visible light-induced efficient contaminant removal by Bi_5O_7I. *Environ. Sci. Technol.* **43**, 2005–2010 (2009).
46. Huang, M. H. *et al.* Room-temperature ultraviolet nanowire nanolasers. *Science* **292**, 1897–1899 (2001).
47. Tian, Q. W. *et al.* Hydrophilic flower-like CuS superstructures as an efficient 980 nm laser-driven photothermal agent for ablation of cancer cells. *Adv. Mater.* **23**, 3542–3547 (2011).
48. Zhang, L. Z. & Yu, J. C. A sonochemical approach to hierarchical porous titania spheres with enhanced photocatalytic activity. *Chem. Commun.* 2078–2079 (2003).
49. Rolison, D. R. Catalytic nanoarchitectures--the importance of nothing and the unimportance of periodicity. *Science* **299**, 1698–1701 (2003).
50. Wang, X. C., Yu, J. C., Ho, C. M., Hou, Y. D. & Fu, X. Z. Photocatalytic activity of a hierarchically macro/mesoporous titania. *Langmuir* **21**, 2552–2559 (2005).
51. Han, L. *et al.* One-pot morphology-controlled synthesis of various shaped mesoporous silica nanoparticles. *J. Mater. Sci.* **48**, 5718–5726 (2013).

Acknowledgments

This work was financially supported by the National Natural Science Foundation of China (Grant Nos. 21377023, 21107013, 21171035, 41073060, and 51272299), Specialized Research Fund for the Doctoral Program of Higher Education (Grant Nos. 20100075110010 and 20110075120012), project of the Shanghai Committee of Science and Technology (13JC1400300), Innovation Program of Shanghai Municipal Education Commission (Grant No. 13ZZ053), the Fundamental Research Funds for the Central Universities and DHU Distinguished Young Professor Program.

Author contributions

L.S.Z. and Z.G.C. designed the experiments. S.J.L. performed the experiments, calculations and data analysis. H.L.W., K.B.X. and J.Q.H. assisted with some of the experiments. Z.G.C., J.S.L. and L.S.Z. guided the work and analysis. S.J.L. and L.S.Z. wrote the paper.

Additional information

Supplementary information accompanies this paper at http://www.nature.com/scientificreports

Competing financial interests: The authors declare no competing financial interests.

How to cite this article: Li, S.J. *et al.* Ta_3N_5-Pt nonwoven cloth with hierarchical nanopores as efficient and easily recyclable macroscale photocatalysts. *Sci. Rep.* **4**, 3978; DOI:10.1038/srep03978 (2014).